# Supporting Information

# Assembling $TiO_2$ nanocrystals into nanotube networks on two dimensional substrates

Yunxin Liu,[a] Shiping Zhan,[c] Jianxin Shi,[b] Qing Peng,*[b] and Yadong Li[b]

[a] *Department of Physics and Electronic science, Hunan University of Science and Technology, Xiangtan 411201, China.*

[b] *Department of Chemistry, Tsinghua University, Beijing 100084, China*

[c] *College of Physics Science and Technology, Central South University, Changsha, 410083, China*

*Email: pengqing@tsinghua.edu.cn

## Part I. Supporting Figures

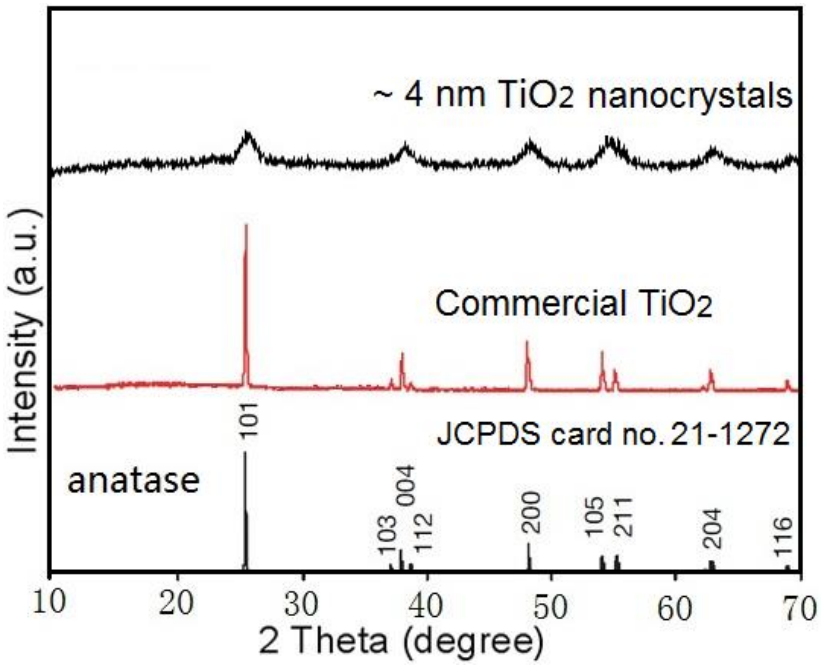


**Figure S1.** XRD spectrum of as-prepared $TiO_2$ nanocrystals.

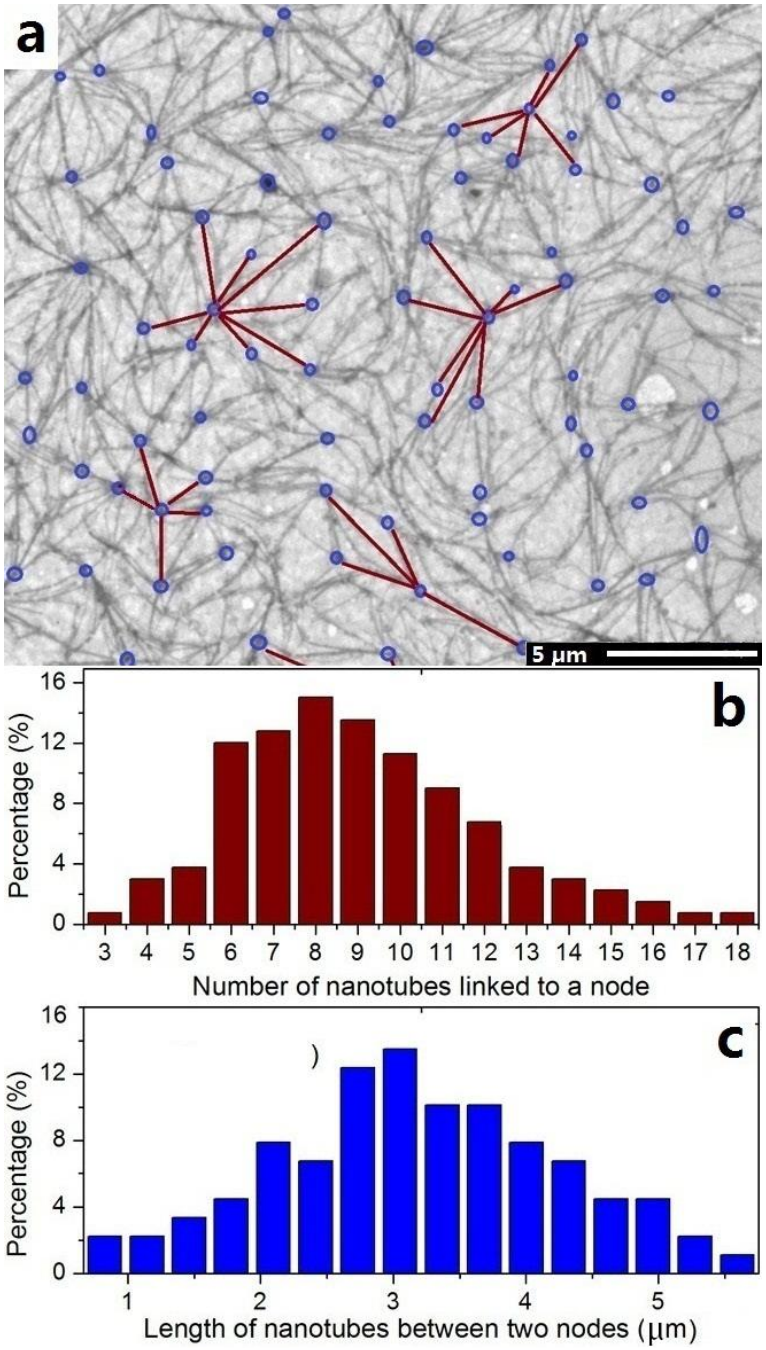


**Figure S2.** The assembled $TiO_2$ nanotube networks on carbon film: (a) every node marked with blue circle and nanotube with deep red line, (b) the number of nanotubes linked to a node, (3) the length of every nanotube between two nodes.

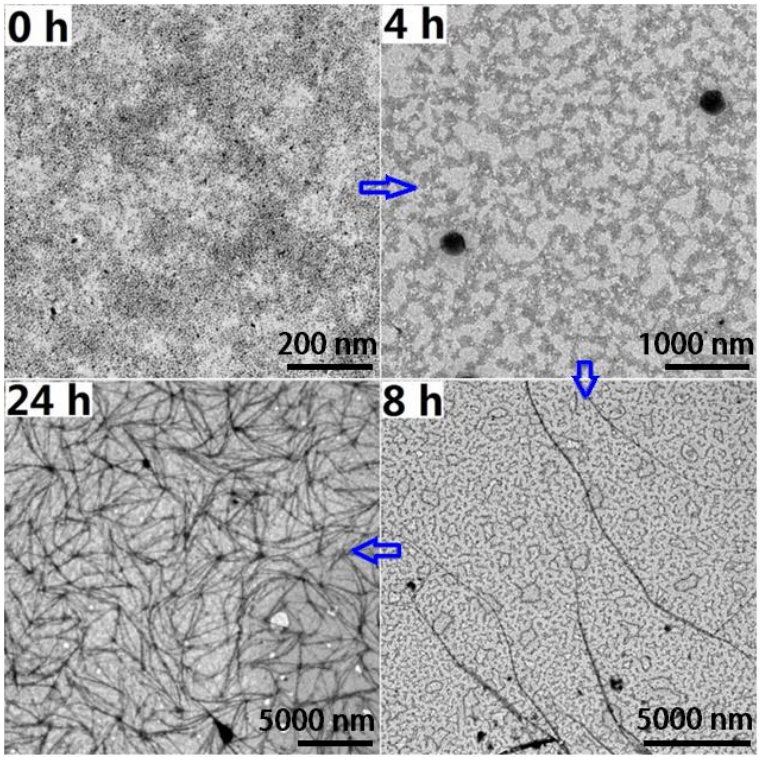


**Figure S3.** TEM images of different assembling stages of $TiO_2$ nanocrystals by ethanol vapor. (a) 0 h, (b) 4 h, (c) 8 h, and (d) 24 h.

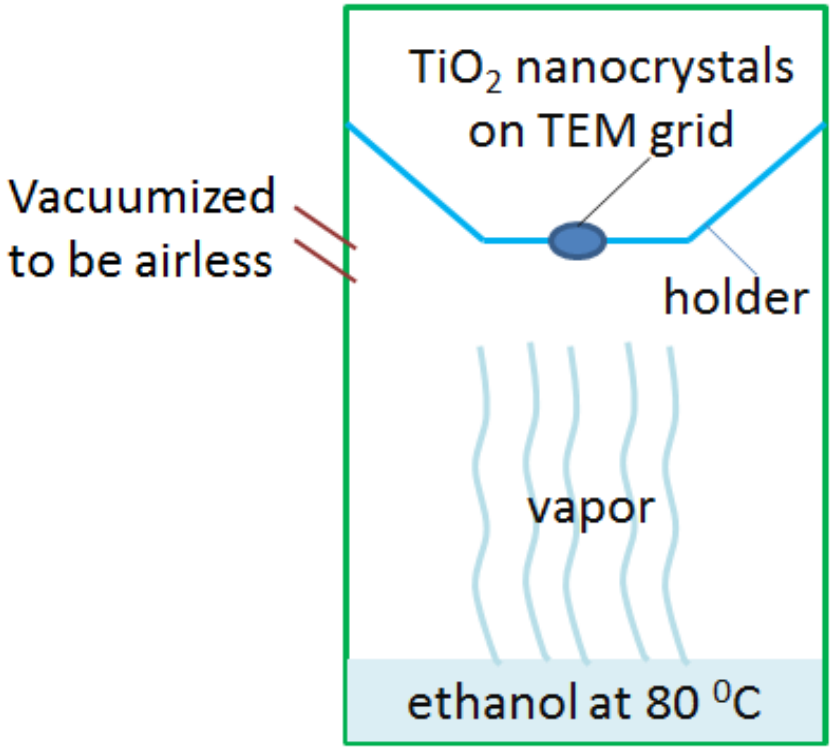


**Figure S4.** A simple model demonstrating the assembly of $TiO_2$ nanocrystals into nanotube networks on carbon film supported by TEM grid.

## Part II. Supplementary discussion

### a) Thermodynamic and kinetic mechanisms in assembly process

Based on the Frenkel-Ladd method developed by Angelani et al,[S1,S2] we can provide a rough assessment of thermodynamic and kinetic factors contributing to the NC assembly process. The equilibrium configuration for a large ensemble of particles can be treated as minimization of the Gibbs free energy ($G$):

$$G = U - TS + PV = H - TS \quad (3)$$

Where $U$ is internal energy, $T$ temperature, $S$ entropy, and H enthalpy. From thermodynamics point of view, the assembly mechanisms will be revealed if the variation of free energy and entropy is addressed. The total entropy $S$ can be decomposed into the sum of a configurational contribution $S_{conf}$ and a vibrational one $S_{vib}$:[S1-4]

$$S = S_{conf} + S_{vib} \quad (4)$$

Herein, it should be noted that $TiO_2$ nanocrystals distribute on the 2D solid substrate instead of in liquid solvent, and directly assemble into nanotube networks under ethanol vapour interaction. Thus, the vibrational entropy $S_{vib}$ contributes to the total one is much less than the configurational entropy $S_{conf}$ and will be roughly taken into account by citing the results for binary hard spheres model. Following, we numerically estimate $S_{conf}$ for $TiO_2$ NC hard spheres.

The method we follow to estimate $S_{conf}$ requires the computation of the total entropy $S$. Via a thermodynamic integration from ideal gas, the total entropy $S$ can also be calculated by Equation (5): [2]

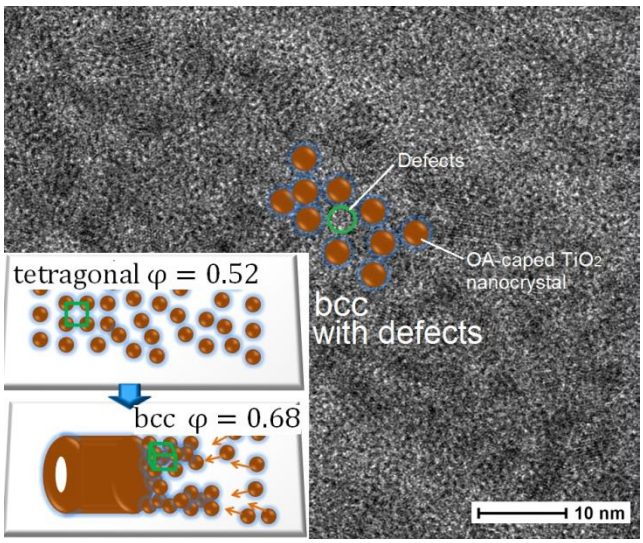


**Figure S5**. HRTEM image of nanotube walls. The packing of oleic acid-caped $TiO_2$ nanocrystals was approximately assigned to body-centered cubic (bcc) with defects for the subsequent simulation calculation of the total, excess, and configuration entropies. The inset: the packing fraction $\varphi$ is equal to 0.52 if the as-prepared TiO2 nanocrystal film is treated as 2D distribution with tetragonal unit. However, this value ($\varphi$) increased to 0.68 after assembly into nanotube networks if the nanotube wall is ascribed to the bcc packing. Considering the defects, we analyzing the systems in the range $\varphi$ = 0.52-0.59.

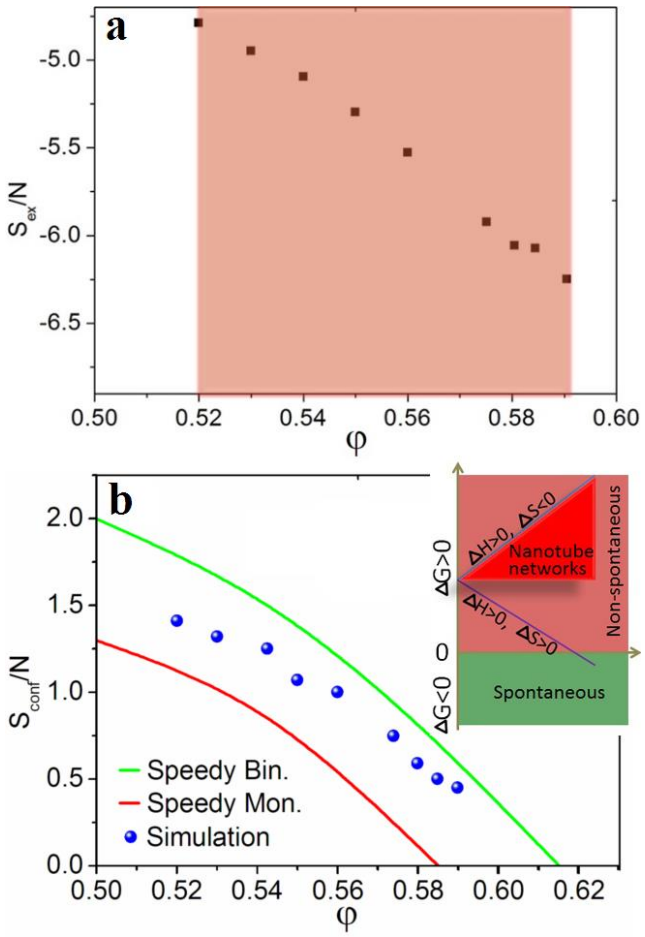


**Figure S6**. a) Excess entropy $S_{ex}$ as function of packing fraction ($\varphi$) for oleic acid-caped $TiO_2$ nanocrystals. obtained from our simulations (symbols). b) Configurational entropy $S_{conf}$ as function of packing fraction $\varphi$. Blue sphere symbols are from our simulation which is compared to the Speedy model for binary (green solid line) and monatomic (red dashed line) hard spheres.

$$S(\rho) = S_{id} + S_{ex}(\rho) \qquad (5)$$

where $S_{id}$ is the entropy of the ideal gas, $S_{ex}$ is the excess entropy with respect to the ideal gas, and $\rho$ is the number density ($\rho = \frac{N}{V}$) which is related to the packing fraction $\varphi$ ($\varphi = \frac{4\pi\rho r^3}{3}$, $r$ radius). In this work, $\varphi$ is approximately

estimated for simplifying the calculation. For a binary mixture, the ideal gas entropy $S_{id}$ is:[S2,S3]

$$S_{id} = \frac{5}{2}N - N\ln(\frac{N}{V}) - 3N\ln\lambda + \ln 2 \quad (6)$$

where $\lambda$ is the De Broglie wavelength and the term *ln2* takes into account the mixing contribution and can be neglected for monatomic hard-spheres. Herein, we consider the superstructure characteristic of the walls of the nanotubes and mainly analyze the systems in the range $\varphi$=0.52−0.59 (Figure 7). The term $S_{ex}$ can be numerically estimated by extracting the excess pressure $P_{ex}$ from the zero density limitation up to the densities of interest (see Figure 8a). Subsequently, the configurational entropy was calculated and shown in Figure 8b. From the simulation results, it could be easily addressed that the configurational entropy decreased in the assembly process of $TiO_2$ nanotube networks ($\Delta S_{conf}$ <0). Considering the predominant contribution of the configurational entropy, it could be easily inferred that the total entropy also decreased ($\Delta S$<0).

Moreover, the internal energy and the effective volume of $TiO_2$ nanocrystals should be constant while the pressure increased in the assembly process due to the ethanol vapor. Then, the total enthalpy should slightly increase ($\Delta H=\Delta PV>0$). According to the variation of Gibbs free energy ($\Delta G=\Delta H-\Delta PV$), it is clear as presented in the inset of Figure 3e that the assembly of $TiO_2$ nanotube networks is not spontaneous which is different from the widely reported nanocrystal superlattices assembly driven by entropy or enthalpy.[S1,S3-8]

**b) Dependences of final structures on the experimental parameters**

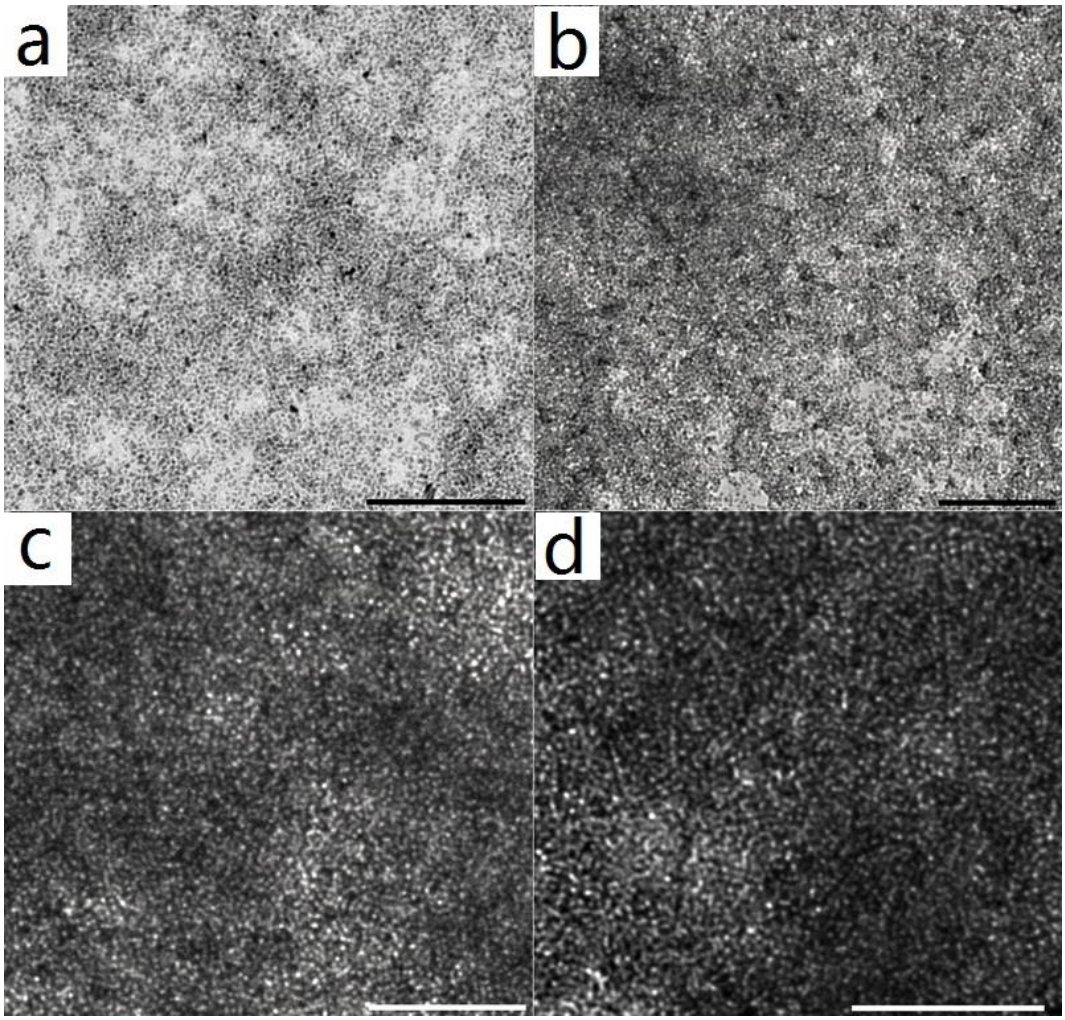


**Figure S7.** TEM images of $TiO_2$ nanocrystal film: a) one monolayer, b) two monolayers, c) three monolayers, and d) four monolayers. The scale bar: 150 nm.

In the practical experiment, we note that the thickness of the deposited $TiO_2$ nanocrystal layer has remarkable influence on the final assembled nanotube networks. $TiO_2$ nanocrystals films with various thicknesses are generated by depositing $TiO_2$ nanocrystals dispersed in cyclohexane on a carbon film supported by TEM grid with $N_2$ flow. The thickness of these films can be roughly and easily controlled by setting the concentration of $TiO_2$ nanocrystals and the $N_2$ flow rate. As shown in **Figure S5**a,

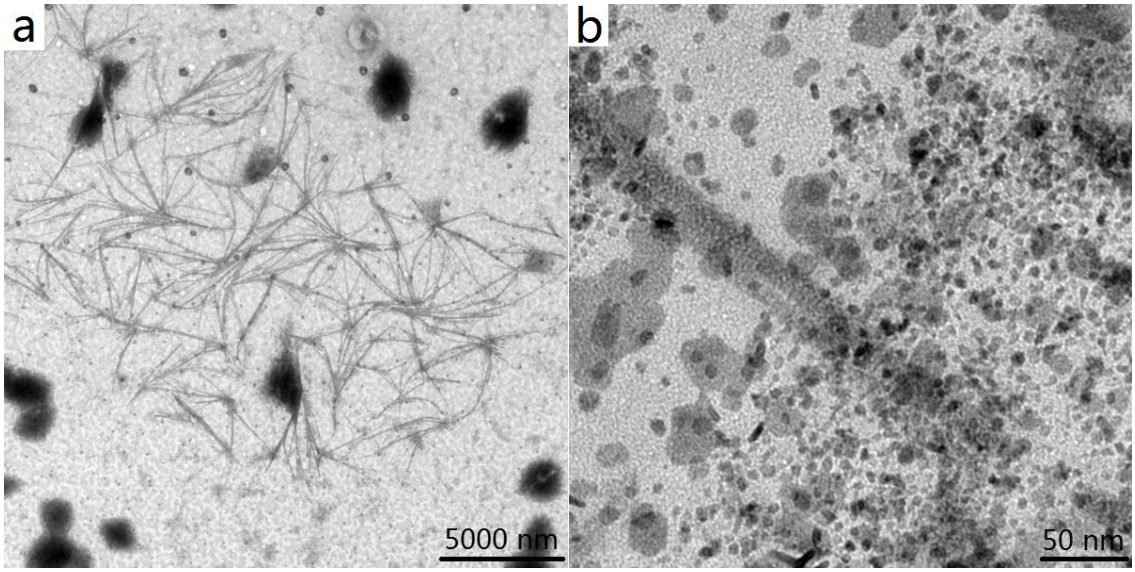


**Figure S8.** TEM images of the assembly of $TiO_2$ nanocrystals with the thickness of a) ~4 monolayers and b) ~6 monolayers.

$TiO_2$ nanocrystal monolayer can form when the concentration of $TiO_2$ nanocrystals is of ~5mg/ml and the $N_2$ flow rate is set as 0.1$Nm^3$/min. The thickness with two and more monolayers can be realized by repeating the one monolayer deposition process. It was observed from Figure S5b-d that $TiO_2$ nanocrystals films with thickness of two to four monolayers have well uniformity at nanoscale. For the assembly of $TiO_2$ nanotube networks, one to three monolayers of $TiO_2$ nanocrystals are suitable for generating nanotube networks with high quality (Figure 1b in main text), while the whole layer thicker than four monolayers leads to the production of an unconnected network with incomplete and fragmented nanotubes (as shown in **Figure S6**). This may be ascribed to a fact that thicker layers have higher systematic degree of disorder. On the other hand, the degree of disorder should be lowered at the process of assembling ordered nanotube networks. Then, it can be reasonably inferred that the assembly of nanotube networks on thick layers of $TiO_2$ nanocrystals is harder than

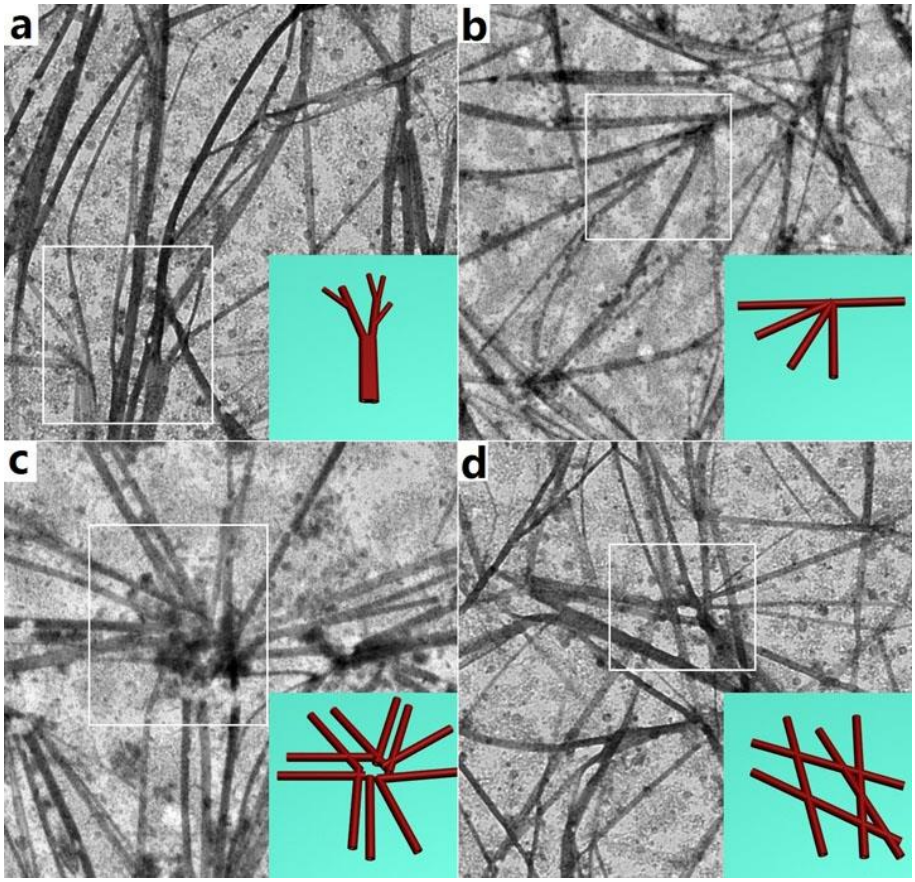


**Figure S9.** TEM images of four types of nodes in the assembled $TiO_2$ nanotube networks.

that on thin ones. In this work, we mainly present a novel method for assembling superstructures inspired by recent reports.[S9-11] The completely revealing of the assembly mechanisms in nanotube networks depends on the further development in experimental, theoretical and calculation works.

In a network, the connection nodes are key components which determine the transmission properties of the whole network. Although the connection nodes in our $TiO_2$ nanotube networks have various morphologies, they can be mainly distributed into four types (see **Figure S7**): the first type belongs a topological structure with large backbones and small limbs; the second one belongs a sector structure in which all nanotubes connect closely in a node; the third one belongs a annular structure; the

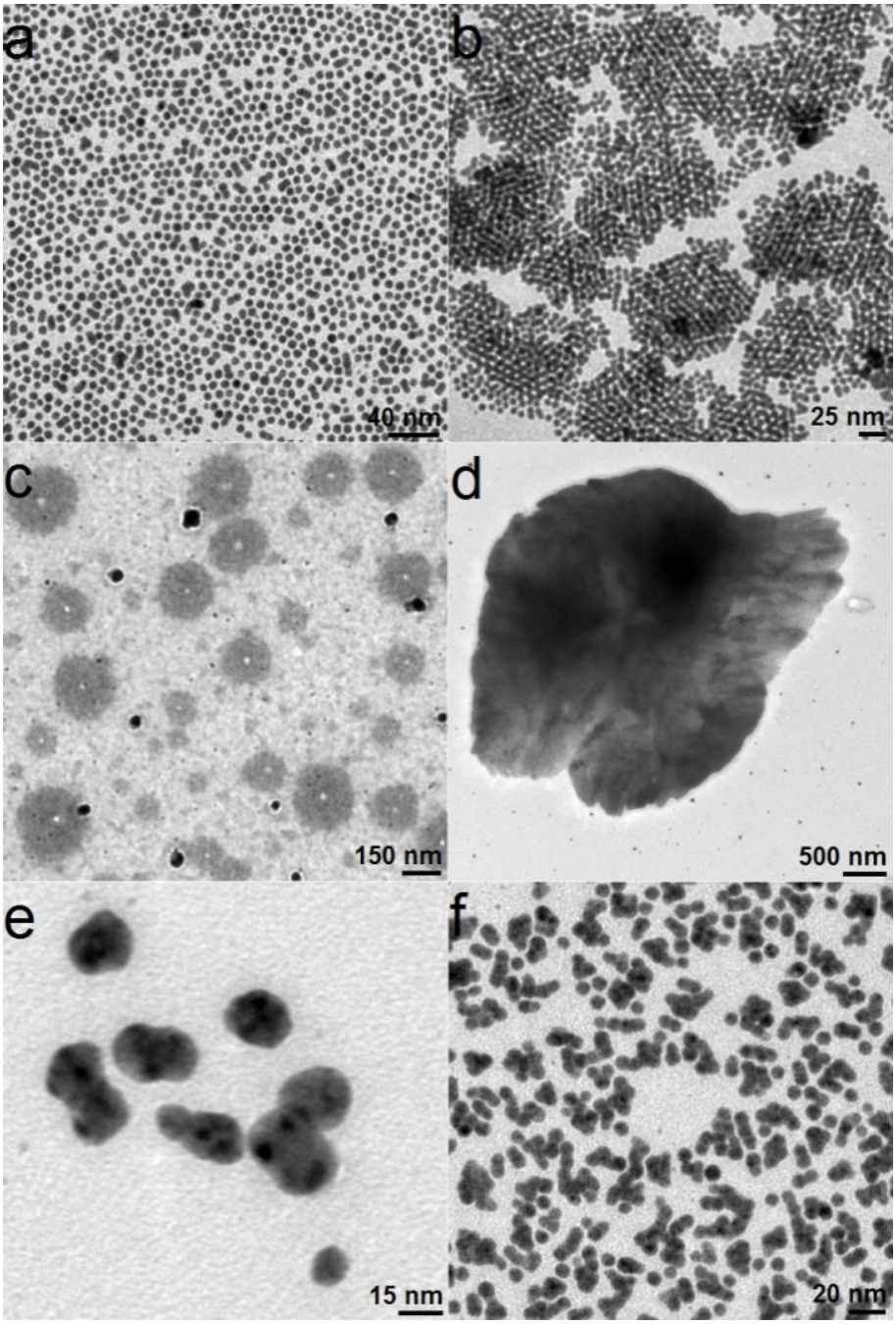


**Figure S10.** The assembly of Ag nanocrystals on carbon film by solvent vapors: (a) as prepared Ag nanocrystals (b) assembled by hexane vapor at 70 $^0$C for 1 h, (c) methanol at 80 $^0$C for 4 h, (d) toluene at 75 $^0$C for 5 h, (e) ethanol at 80 $^0$C for 2h, and (f) tetrahydrofuran at 68 $^0$C for 3 h.

forth one is a simple cross structure in which two nanotubes cross with each other with random nodes. It should be noted that the first, second, and forth types of nodes had well connectivity while the third one did not link well with each other to ensure

the good connectivity. It may be reasonable to regard the third type as open-framework nodes, which can be used as the potential node linking with the external electrodes. The relative ratio of four types of nodes can be tuned by changing the synthetic conditions. However, a large number of nodes should be counted for a $TiO_2$ networks which requires a longer research period and under way in our labs. Solvent vapor is also powerful for driving the assembly of metal nanocrystals into superstructures. **Figure S8** shows that oleic acid-caped Ag nanocrystals can be assembled into 2D superlattice grains, hollow discs, micrometer-scale sheets, dumbbells, and short chains by different solvent vapors. These structurally intricate Ag superstructures also supply Hanrath's conclusion with experimental evidences that the solvent-ligand interaction plays a main role for the assembling processes of ligand caped nanocrystals by solvent vapor, instead of the electrostatic couple-couple interaction which is powerless for controlling the nanocrystal building blocks to assemble so many types of intricate superstructures. It should be pointed out that although the assembly mechanisms related to solvent vapor can be elucidated based on Hanrath's model at molecular grade, the physical and chemical processes at the atomic grade are still unrevealed which may be resolved with the development of in situ observation of the growth and assembly processes of nanocrystals.[S12,S13] In our investigation, UV-VIS spectrum was firstly considered and selected as the technical way to probing the structural variation from $TiO_2$ NCs to Nanotube networks. But, the detectable signal is very weak and no obvious bandgap absorption shift was observed (see Figure S11).

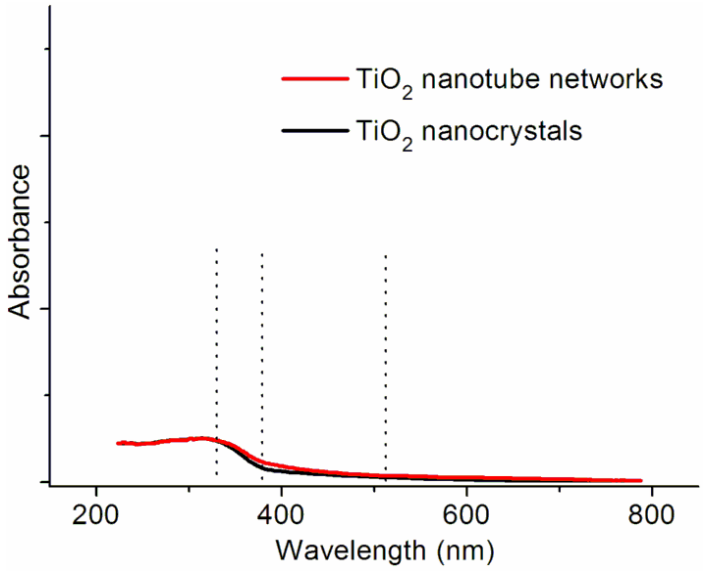


**Figure S11.** UV-Vis spectrum of as-prepared $TiO_2$ nanocrystals and the assembled $TiO_2$ nanotube networks.

**Supplementary References**

[S1] D. Frenkel, B. M. Mulder, J. P. McTague, Phys. Rev. Lett. 1984, **52**, 287.

[S2] L. Angelani, G. Foffi, J. Phys.-Condens. Matter 2007, **19**, 256207.

[S3] M. I. Bodnarchuk, M. V. Kovalenko, W. Heiss,, Dmitri V. Talapin, J. Am. Chem. Soc. 2010, **132**, 11967.

[S4] M. D. Eldridge, P. A. Madden, D. Frenkel, Mol. Phys. 1993, **79**, 105.

[S5] E. V. Shevchenko, D. V. Talapin, N. A. Kotov, S. O'Brien,, C. B. Murray, Nature 2006, **439**, 55.

[S6] D. V. Talapin, E. V. Shevchenko, C. B. Murray, A. V. Titov,, Petr Král, Nano Lett. 2007, **7**, 1213.

[S7] J. Henzie, M. Grünwald, A. Widmer-Cooper, P. L. Geissler,, P. D. Yang, Nat. Mater. 2012, **11**, 131.

[S8] I. Florea, A. Demortière, C. Petit, H. Bulou, C. Hirlimann,, O. Ersen, ACS Nano 2012, **6**, 2574.

[S9] B. W. Goodfellow, B. A. Korgel, ACS Nano 2011, **5**, 2419.

[S10] T. Hanrath, J. J. Choi, D. M. Smilgies, ACS Nano 2009, **3**, 2975.

[S11] K. Bian, J. J. Choi, A. Kaushik, P. Clancy, D. M. Smilgies, T. Hanrath, ACS Nano 2011, **5**, 2815.

[S12] H. M. Zheng, R. K. Smith, Y. Jun, C. Kisielowski, U. Dahmen and A. P. Alivisatos, Science 2009, **324**, 1309.

[S13] H. M. Zheng, J. B. Rivest, T. A. Miller, B. Sadtler, A. Lindenberg, M. F. Toney, L. W. Wang, C. Kisielowski and A. P. Alivisatos, Science 2011, **333**, 206.